In-Silico nanomedical exploration of mefloquine drug transport using pegylated graphene oxide nanocarrier.

ADVANCED THEORY AND SIMULATIONS
www.advtheorysimul.com

In-Silico Nanomedical Exploration of Mefloquine Drug Transport Using Pegylated Graphene Oxide Nanocarrier

Oluwasegun Chijioke Adekoya, Gbolahan Joseph Adekoya, Emmanuel Rotimi Sadiku, and Yskandar Hamam*

This study investigates the *in-silico* transport of mefloquine (MQ) by using graphene oxide (GO) and polyethylene glycol (PEG)-functionalized GO nanocarriers. Density functional theory (DFT) calculations are performed to explore the molecular interactions, electronic properties, thermodynamics, and release kinetics of MQ-GO and MQ-GO/PEG complexes across different phases and environmental conditions. Results indicate a strong affinity between MQ and both types of nanocarriers, with the adsorption energies ranging from −59.14 to −143.16 kcal mol^{-1}, particularly in acidic environments. This suggests a potential for targeted drug delivery in acidic tumor micro-environments. The incorporation of PEG, enhances stability and compatibility across phases, with chi interaction parameters of between 1.36 and 28.47, and the energy of mixture values, ranging from 0.80 to 16.86 kcal mol^{-1}. The release time of MQ from the nanocarriers, varies significantly, depending on the adsorption energy, and ranges from 2.03 × 10^{30} to 6.98 × 10^{91} milliseconds across different phases, highlighting the need for further optimization of the drug delivery systems. The findings of this study provide valuable insights into the design and development of novel nanomedicines, based on MQ and GO nanocarriers, with implications for malaria treatments.

1. Introduction

The burgeoning field of nanomedicine has witnessed groundbreaking advancements at the intersection of materials science and pharmaceutical research, particularly in the development of innovative drug delivery systems.[1] This research, endeavors to delve into the intricate realm of nanotechnology by focusing on the *in-silico* exploration of mefloquine (MQ) in, a potent anti-malarial drug, facilitated through a nanocarrier that is composed of graphene oxide (GO) and polyethylene glycol (PEG). The strategic amalgamation of these cutting-edge materials holds the promise of enhancing therapeutic efficacy while mitigating the undesirable side effects that are associated with conventional drug delivery methods.

MQ, characterized by its diverse pharmacological properties, has emerged as a compelling candidate for repurposing in the existence of evolving global health challenges. Despite challenges, e.g., the resistance of emergence and neuropsychiatric side effects, MQ stands as a valuable treatment option for falciparum malaria. This necessitates a judicious approach, prompting the cautious use and exploration of the potential combinations with other antimalarial agents.[2]

Recent investigations have spot-lighted the use of MQ, as a promising candidate for addressing the ongoing challenges, posed by COVID-19, particularly in the sub-Sahara African regions. Its potential as an effective entry inhibitor since SARS-CoV-2 positions it as a viable option for COVID-19 treatment. To address the challenges associated with bioavailability and

O. C. Adekoya, G. J. Adekoya, E. R. Sadiku
Institute of Nanoengineering Research (INER) & Department of Chemical
Metallurgical and Materials Engineering
Faculty of Engineering and the Built Environment
Tshwane University of Technology
Pretoria 0001, South Africa
E-mail: 222532949@tut4life.ac.za

Y. Hamam
Department of Electrical Engineering
Faculty of Engineering
and the Built Environment
Tshwane University of Technology
Pretoria 0183, South Africa

Y. Hamam
École Supérieure d'Ingénieurs en Électrotechnique et Électronique
Cité Descartes
2 Boulevard Blaise Pascal, Noisy-le-Grand, Paris 93160, France

The ORCID identification number(s) for the author(s) of this article can be found under https://doi.org/10.1002/adts.202400461

DOI: 10.1002/adts.202400461

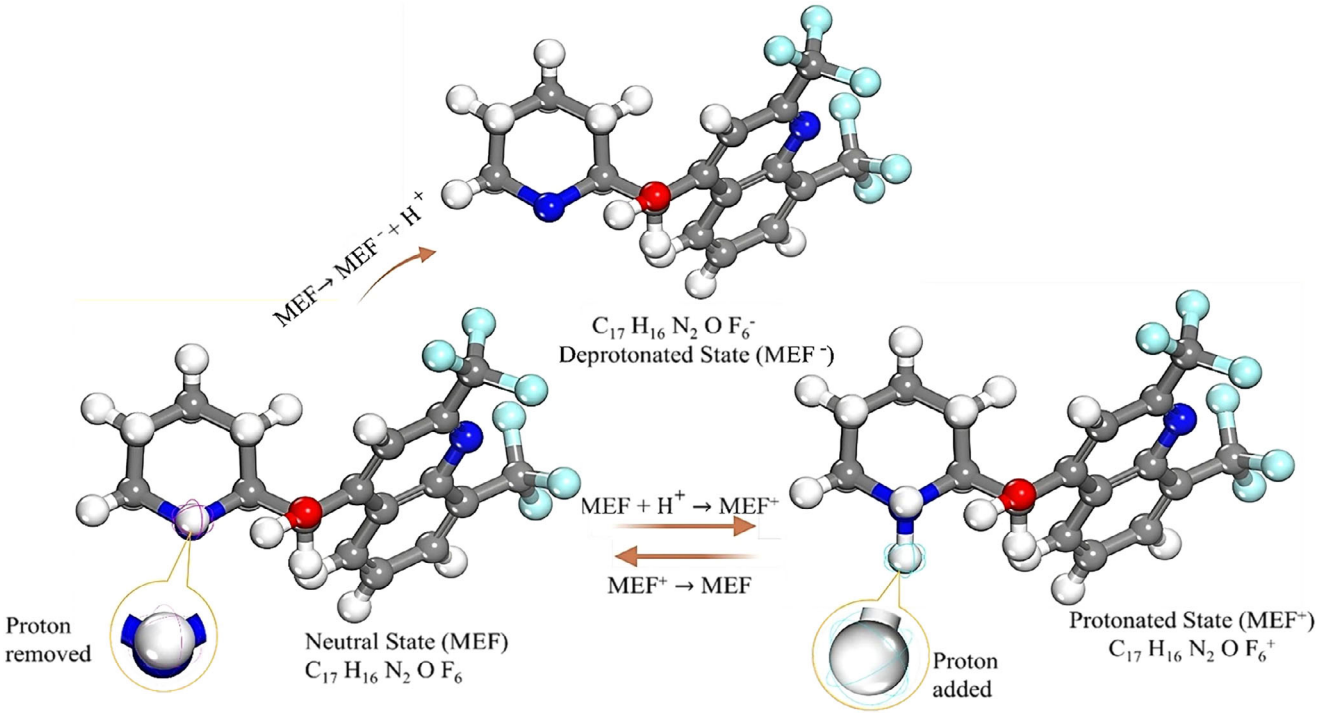

Figure 1. Optimized 3D molecular structures of mefloquine (MQ) in its neutral and protonated states, visualized with distinct color representation for oxygen (red), carbon (grey), hydrogen (white), fluorine (pale turquoise), and nitrogen (blue), offering detailed insight into molecular conformation, deprotonation, and protonation dynamics.

side effects at higher doses, researchers are exploring innovative approaches, including the incorporation of polymeric nanocarriers, such as graphene oxide-reinforced poly(lactic-*co*-glycolic) acid (PLGA), to optimize drug delivery systems.[4]

The incorporation of nanocarriers, specifically engineered with nanomaterials, e.g., graphene oxide, and biocompatible polymers, e.g., polyethylene glycol, emerges as a promising route to address the existing challenges in drug delivery.[5] The versatility of PEG-GO nanocomposites as drug carriers has been highlighted across various therapeutic applications, showcasing their controlled release capabilities. Researchers have explored the potentials of PEG-GO nanocomposites in controlled drug release for antibiotics, anticancer therapeutics, and other medical applications, hence, underscoring their versatility.[6] For instance, Huiyun et al.,[7] focused on overcoming the drug release barriers, posed by PEGylation through the development of a redox-responsive PEG detachment mechanism in PEGylated nano-GO, resulting in rapid drug release at tumor-relevant glutathione levels for enhanced intracellular delivery.[7] Similarly, Mohamad et al.,[8] synthesized a PEG-functionalized GO nanohybrid for efficient loading and pH-sensitive release of doxorubicin, demonstrating its potential applications in cancer treatment.[8] These studies collectively, highlight the versatility and promise of PEG-GO nanocomposites as drug carriers with applications ranging from antibiotics to anticancer therapeutics, showcasing their controlled release capabilities and their potential for targeted drug delivery systems.[9]

The purpose of this *in-silico* exploration is to predict and understand the interactions between the drug, nanocarrier, and biological environments at the molecular level. The Density Functional Theory (DFT), emerges as a pivotal tool for investigating drug delivery systems, offering insights into the molecular interactions and design strategies.[10] The comprehensive review by Adekoya and co-authors,[11] highlighted the increasing application of the DFT in designing polymer-based drug delivery systems, emphasizing its role in predicting the essential characteristics and providing a glimpse into the future trends in the field.

Therefore, through the simulation of the dynamic interplay within the MQ-loaded GO/PEG nanocarrier system, this investigation aims to clarify certain crucial parameters. These include drug release kinetics, nanocarrier stability, and electronic and thermodynamic interactions with the drug. Besides, acknowledging the pH-dependent drug release, a mechanism proposed by Hazrati et al., was considered.[12] The acidic environment within the COVID-infected cells and the alkaline pH of specific bodily channels require consideration for the protonation and deprotonation of MQ (**Figure 1**). The data obtained, contribute valuable insights for the required rational design of the next-generation nanocarriers, with potential applications reaching beyond malaria treatment **Figure 2**.

2. Computational Method

The research methodology employed in this investigation comprises various essential stages: optimization of molecular structures, assessment of energetic attributes, scrutiny of non-covalent interactions, computation of theoretical infrared (IR) and ultraviolet (UV) spectra, and the evaluation of the

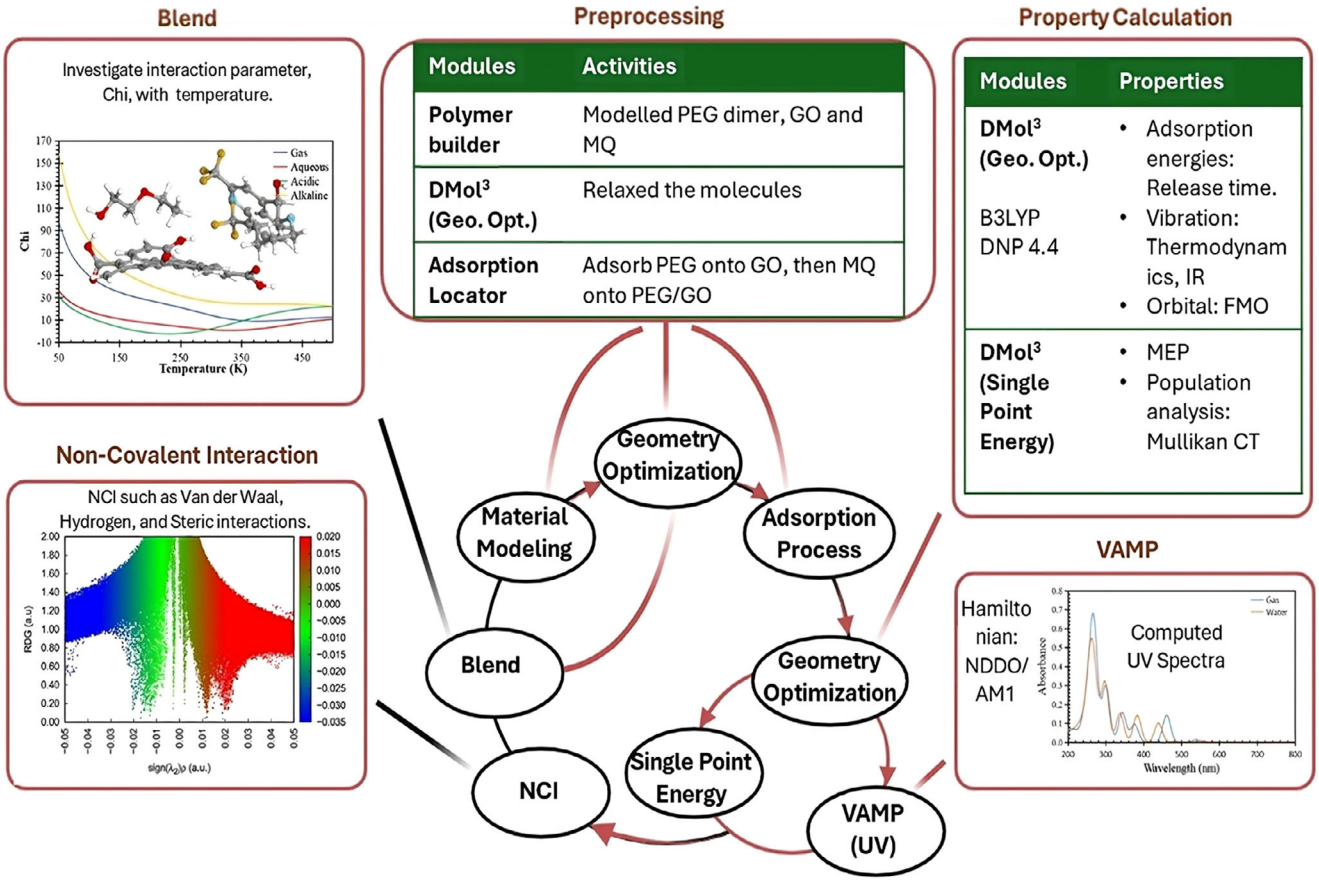

Figure 2. Integrated workflow analysis of mefloquine drug transport by using PEGylated GO nanocarrier: unveiling intermolecular dynamics and mechanistic insights.

release kinetics and the thermodynamic features of the complexes. Figure 2 illustrates a schematic representation of the computational approach.

To fabricate the nanocarrier, a simulation for adsorption was executed by involving a dimer, comprising of PEG and 3 × 2-GO.[6a] The GO nanosheet was structured with two −OH terminations and two COOH terminals at its peripheries.[6a,13] By utilizing the DMol^3 module within Materials Studio 2020 software,[14] the configurations of GO, PEG, and the MQ drug molecule were optimized by employing the B3LYP exchange–correlation method, with the DNP 4.4 basis set. The optimization process included the integration of a long-range dispersion correction via the Grimme method. Geometry convergence tolerances and electronic self-consistent field (SCF) tolerance were meticulously set to ensure precision.

The methodology employed diverse environmental simulations, including aqueous, acidic, and alkaline conditions, utilizing the Conductor-Like Screening Model (COSMO) within the DMol^3 computational framework. COSMO encapsulates solute molecules within a dielectric medium, simulating solvation effects on the complex stability. For the simulation of the aqueous environments, water solvent with a dielectric constant of 78.54, was chosen.[15] The protonation and deprotonation of MQ consider the secondary amine nitrogen (-NH-), due to its high basicity, as shown in Figure 1.[16]

Moreover, the adsorption computation, needed to identify the most energetically favorable configuration, was conducted by using the Adsorption Locator module, employing the Monte Carlo method to explore the various configurational spaces. Single-point energy calculations by using the DMol^3 module, were employed to assess the energetic attributes and the molecular descriptors.[14] Subsequently, the release kinetics and the thermodynamic characteristics of the complexes were determined. Non-covalent interactions were scrutinized by utilizing the Multiwfn software,[17] with the necessary visualization, facilitated by Visual Molecular Dynamics (VMD) software.[18] Mulliken analysis was utilized to assess the charge transfer, while the UV optical spectra computation, in both the gas and aqueous phases, providing critical data, such as the: oscillator strength and excitation energies under visible light, was performed by using the Visualisation and Analysis of Molecular Properties (VAMP) module.[19]

3. Results and Discussion

3.1. Interaction of GO/PEG NCs with MQ

3.1.1. Adsorption Energies

The interaction between the MQ drug and GO/PEG nanocarriers was evaluated by computing the adsorption energies (E_{ad}) across

Table 1. Adsorption Energies, Distances, Charge Transfer, and Release Time of MQ-Nanocomposite Complexes across Different Phases.

Species	Phases	E_{ad} (Kcaℓ/moℓ)	D (Å)	Adsorption site	Q (e)	Chi (298 K)	E_{mix} (298 K)	τ (ms)
MQ-GO NCs	gas	−117.33	1.88	H → O	−0.035	26.12	15.47	8.37×10^{72}
	water	−108.52	1.82	H → O	−0.020	9.50	5.62	2.96×10^{66}
	acidic	−143.16	1.50	N → H	0.500	15.01	8.89	6.98×10^{91}
	Alkaline	−101.17	2.50	H → H	−0.144	28.47	16.86	1.23×10^{61}
MQ-GO/PEG NCs	gas	−66.73	1.71	N → H	0.034	14.43	8.55	7.38×10^{35}
	water	−59.14	1.58	N → H	0.072	1.36	0.80	2.03×10^{30}
	acidic	−104.87	1.67	H → O	0.769	6.59	3.90	6.29×10^{63}
	Alkaline	−76.54	2.10	F → H	0.116	26.54	15.71	1.13×10^{43}

various phases, including the: gas, aqueous, acidic, and alkaline environments. Notably, significant variations in the adsorption energies were observed, indicating diverse interaction strengths and potential application scenarios.

The adsorption energies (E_{ad}) and adsorption distances (d) of MQ on both the GO and PEGylated GO nanosheets were calculated across the various phases: gas, aqueous, acidic, and alkaline environments (Equations 1 and 2).[20] The results, summarized in **Table 1**, offer critical insights into the efficacy of drug delivery under various conditions.

$$E_{ad} = E_{\mathrm{GPF}} - \left(E_{\mathrm{MQ}} + E_{\mathrm{GO/PEG}}\right) \quad (1)$$

$$E_{DFT-D} = E_{DFT} + E_{Disp} \quad (2)$$

In these equations, E_{GPF}, E_{MQ} and $E_{\mathrm{GO/PEG}}$ denote the energies of the drug-excipient system, the drug molecule, and the nanocarrier, respectively. Additionally, E_{Disp} as proposed by Grimme, denotes the long-range dispersion correction energy.[21]

In the gas phase, MQ exhibited a strong affinity toward GO/PEG nanocarriers, with an adsorption energy of −117.33 kcal moℓ$^{-1}$, indicative of robust drug-carrier interactions. This trend persisted in the acidic media, where the adsorption energy peaked at −143.16 kcal moℓ$^{-1}$, underscoring the favorable binding of MQ to GO/PEG in acidic conditions. Conversely, in the aqueous and alkaline environments, the adsorption energies were comparatively, lower (−108.52 and −101.17 kcal moℓ$^{-1}$, respectively), yet still substantial, signifying the versatility of GO/PEG nanocarriers in different physiological environments. For instance, when comparing the adsorption energies of hydroxychloroquine with various nanotubes, *viz*: Aluminum-Doped Nanotubes (Aℓ-CNT) exhibit −45.07 and −43.02 kcal moℓ$^{-1}$ in both the gas and aqueous phases, Silicon-Doped Nanotubes (Si-CNT) show −15.78 and −14.43 kcal moℓ$^{-1}$ in both phases and silicon Carbide Nanotubes (SiC-NT) display −45.15 and −43.86 kcal moℓ$^{-1}$ in both phases. However, GO and PEGylated GO, demonstrate the highest adsorption energy for MQ among these nanocarriers, indicating their potential as carriers for drug delivery.[22]

The adsorption distances (d) of MQ from the carriers were also assessed, revealing compact configurations across all phases, with distances ranging from 1.50 to 2.50 Å. This proximity suggests intimate drug-carrier associations, that are conducive to efficient drug delivery and release mechanisms. **Figure 3** illustrates the optimized 3D structures, interaction distances, and adsorption energies of the MQ-GO/PEG NCs complex across different phases.

The variations observed in the adsorption energies highlight the sensitivity of drug-carrier interactions to environmental factors, which are crucial for the tailoring of drug delivery systems to specific physiological conditions. The pronounced affinity of MQ toward GO/PEG nanocarriers, particularly in acidic environments, suggests its potential applications in targeted drug delivery to acidic tumor microenvironments, where conventional drug delivery systems often falter.

Furthermore, the compact configurations of MQ on GO/PEG nanocarriers imply enhanced stability and reduced drug leakage during transit, which is essential for maintaining therapeutic efficacy. These findings contribute to a deeper understanding of MQ delivery mechanisms by using GO/PEG NCs across diverse phases, paving the way for the development of optimized drug delivery platforms with enhanced bioavailability and targeted delivery capabilities.

3.1.2. Electrostatic Interactions and Charge Transfer Analysis

The electrostatic interactions and the charge transfer analysis provide crucial insights into the behavior of the Mefloquine (MQ) drug when interacting with PEGylated GO nanocarriers in different environments. These findings are pivotal for the understanding of the dynamics of drug delivery systems, particularly in the context of enhancing therapeutic efficacy and bioavailability, which are vital considerations in combating diseases, e.g., COVID-19.

In the gas phase, the MQ-GO/PEG NCs complex, exhibits a slight negative charge [Q(e) = −0.035], while the GO/PEG complex alone, shows a small positive charge [Q(e) = 0.034]. This indicates a weak interaction between MQ and the nanocarrier in this phase, possibly due to the minimal solvent effects or intermolecular interactions.

Transitioning to the aqueous phase, the charge transfer dynamics shift, with the MQ-GO/PEG NCs acquiring a slightly less negative charge [Q(e) = −0.020] when compared to the gas phase. Conversely, the MQ-GO/PEG NCs complex experiences an increase in positive charge [Q(e) = 0.072], in the presence of water. These changes suggest a more favorable interaction between MQ and the nanocarrier in an aqueous environment, possibly due to solvation effects that enhance electrostatic interactions.

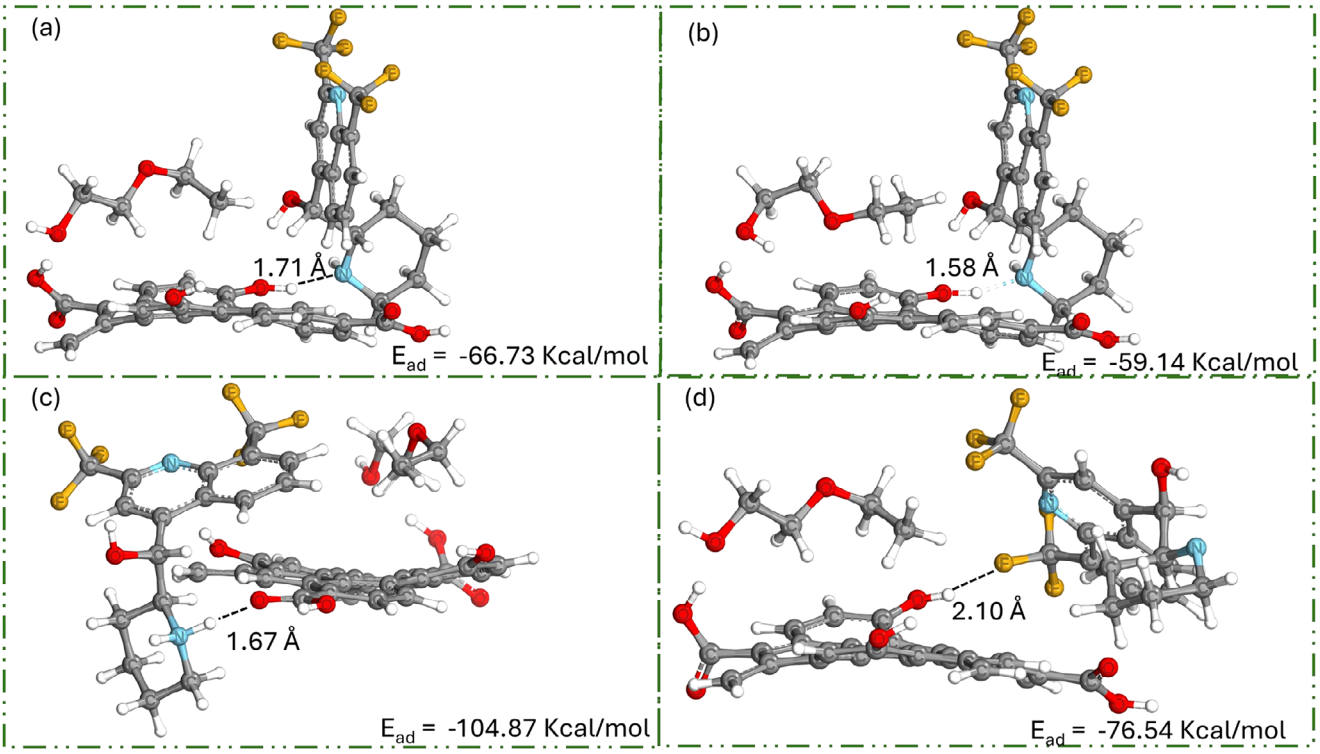

Figure 3. Displays of the: optimized 3D structures, interaction distances, and adsorption energies of the MQ-GO/PEG NCs complex across the different phases, *viz*: a) gas, b) aqueous, c) acidic, and d) alkaline environments.

In acidic conditions, the charge transfer behavior undergoes a significant alteration. The MQ-GO/PEG NCs complex, exhibits a substantial positive charge [Q(e) = 0.500], indicating a pronounced interaction between the drug and the nanocarrier. This is attributed to the protonation of specific functional groups on MQ and/or the nanocarrier under acidic conditions, leading to strong electrostatic interactions and charge transfer.

Conversely, in alkaline environments, the MQ-GO/PEG NCs complex displays a moderately negative charge [Q(e) = −0.144]. This contrasts with the positive charge observed in acidic conditions, suggesting a reversal of charge transfer dynamics, influenced by the pH environment. The alkaline conditions are believed to deprotonate certain functional groups, affecting the overall charge distribution and interaction strength between MQ and the nanocarrier.

The molecular electrostatic potential maps, depicted in **Figure 4** and Figure S2 (Supporting Information), provide a visual confirmation of these charge transfer dynamics, showing how the distribution of positive and negative electrostatic potentials, varies across different phases and configurations. Specifically, the concentration of the negative potentials around oxygen and fluorine atoms of both the drug and the carriers, and positive potentials around the carbon and hydrogen atoms, highlights the key regions involved in the electrostatic interactions.

These findings hold significant implications for mefloquine delivery when utilizing PEGylated GO nanocarriers, especially in the context of antiviral treatment. The ability to modulate charge transfer and electrostatic interactions, based on environmental conditions, opens suitable avenues for precise control over drug release kinetics and targeting, thereby potentially, enhancing therapeutic outcomes while minimizing adverse effects. Furthermore, the understanding of the impact of the pH on charge transfer, provides insights into the optimization of drug delivery systems for specific physiological conditions, e.g., the acidic microenvironment of inflamed tissues or the alkaline condition, often encountered during disease progression.

3.1.3. Non-Covalent Interaction (NCI) of the MQ Drug-GO Nanocarrier Systems

The non-covalent interaction (NCI) analysis provides valuable insights into the binding mechanisms between MQ drug molecules and GO nanocarriers, both with and without PEGylation, across various phases and environmental conditions. The understanding of these interactions is crucial for elucidating the mechanisms underlying MQ delivery by utilizing PEGylated GO nanocarriers and exploring their potential implications for antiviral treatment.

The reduced density gradient (RDG) analysis, facilitated by Equation 3, offers a quantitative assessment of the electron density ($\rho(r)$) distribution and the strength of the non-covalent interactions within the optimized complexes. The visual representations, provided by the RDG isosurface maps and the scatter plots, aid in the interpretation of the nature and the significance of these interactions (**Figures 5** and **6**, Figures S3 and S4,

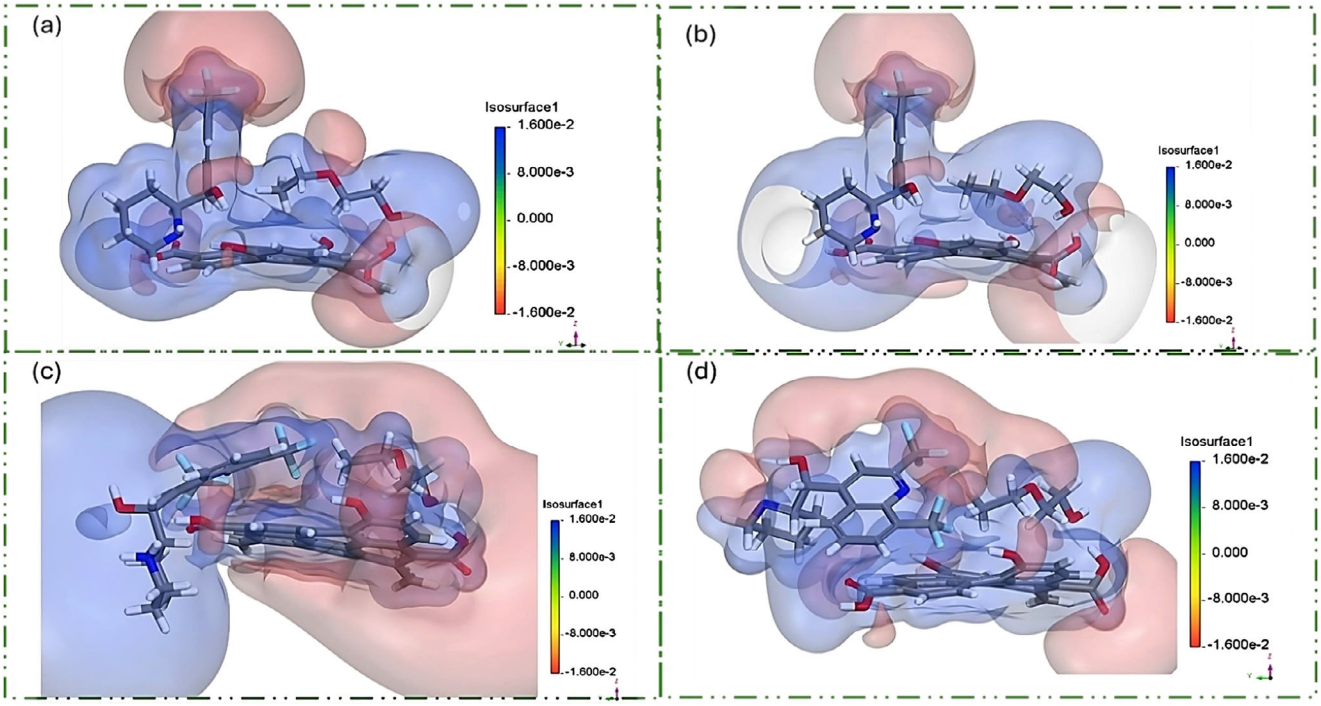

Figure 4. Molecular electrostatic potential mapping illustrating the optimized interaction of the MQ-GO/PEG NCs complex in diverse phases: a) gas, b) aqueous, c) acidic, and d) alkaline environments, unveiling the spatial distribution of electrostatic charges critical for understanding intermolecular interactions and stability across different environmental conditions.

Supporting Information).

$$RDGs = \frac{1}{2(3\pi^2)^{\frac{1}{3}}} \frac{\left|\overline{\Delta\rho}(r)\right|}{\overline{\rho(r)}^{\frac{4}{3}}} \tag{3}$$

In the gas phase, both the MQ-GO NCs and MQ-GO/PEG NCs complexes exhibit distinct non-covalent interactions. The MQ-GO NCs complex, demonstrates a weak hydrogen bonding between hydrogen and oxygen atoms, with a binding energy (E_{ad}) of −117.33 kcal moℓ^{-1}, suggesting a moderate affinity. Conversely, the MQ-GO/PEG NCs complex shows a stronger hydrogen bonding between nitrogen and hydrogen atoms, indicating a more robust interaction, with an E_{ad} of −66.73 kcal moℓ^{-1}.

In the transitioning to the aqueous phase, both complexes maintain weak hydrogen bonding interactions, *albeit*, with slightly reduced binding energies when compared to the gas phase. This suggests that the presence of water molecules influences the strength of the hydrogen bonding interactions between MQ and the nanocarriers.

Under acidic conditions, the nature of non-covalent interactions undergoes significant changes. The MQ-GO NCs complex experiences the van der Waals interactions between nitrogen and hydrogen atoms, indicating a stronger binding affinity when compared to hydrogen bonding. In contrast, the MQ-GO/PEG NCs complex exhibits a strong hydrogen bonding between the hydrogen and oxygen atoms, suggesting a preferential interaction under acidic conditions.

In alkaline environments, both complexes engage primarily in van der Waals interactions, *albeit*, with differing adsorption sites and strengths. The MQ-GO NCs complex demonstrates the existence of van der Waals interactions between hydrogen atoms, while the MQ-GO/PEG NCs complex exhibits the existence of van der Waals interactions between fluorine and hydrogen atoms.

These findings enhance our comprehension of MQ delivery by using PEGylated GO nanocarriers across different phases and environments. The prevalence of hydrogen bonding and van der Waals interactions highlights the importance of intermolecular forces in stabilizing the complexes and facilitating drug delivery. Moreover, the variation in non-covalent interactions, under different pH conditions, underscores the importance of environmental factors in modulating drug-nanocarrier interactions and ultimately, influences the therapeutic efficacy.

3.2. Miscibility Study of the MQ Drug-GO Nanocarrier Systems

In the pursuit of elucidating the efficacy and feasibility of employing PEGylated GO nanocarriers for the transportation of MQ, a comprehensive miscibility study was conducted across various media. The study was aimed at assessing the interactions between MQ drug molecules and the GO nanocarriers, with and without PEGylation in the gas, aqueous, acidic, and alkaline environments. The results obtained, as detailed in Table 1, provide crucial insights into the compatibility and the potential applicability of these nanocarrier systems in different phases.

First, it is noteworthy that the chi (χ) interaction parameter serves as a measure of miscibility, with high values, indicating strong intermolecular interactions and hence, good miscibility.

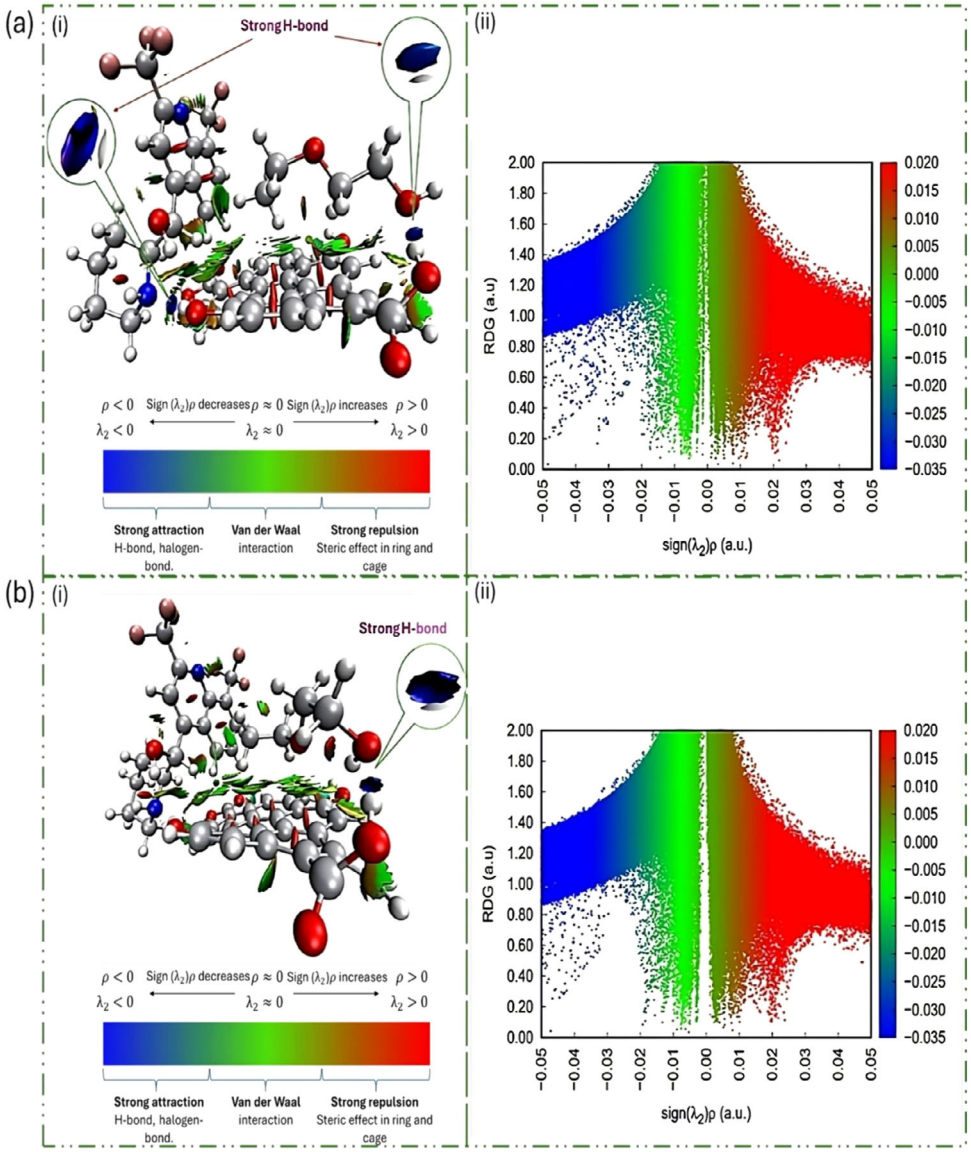

Figure 5. Exploration of the noncovalent interactions within the optimized MQ-GO/PEG NCs complex via the RDG isosurface mapping (left) and the scatter plot analysis (right) across: a) gas and b) aqueous phases, offering an insight into the intermolecular forces and the molecular recognition patterns.

Additionally, the energy-of-mixture (E_{mix}), reflects the overall stability of the MQ drug-GO nanocarrier complexes, with low values, suggesting great stability.

$$E_{mix} = \frac{1}{2} z \left(E_{bs} + E_{sb} - E_{bb} - E_{ss} \right) \quad (4)$$

In the gas phase, both the MQ-GO NCs and MQ-GO/PEG NCs complexes exhibited relatively high chi values of 26.12 and 14.43, respectively. This suggests favorable interactions between MQ and GO nanocarriers, indicative of good miscibility. The corresponding E_{mix} values of 15.47 for MQ-GO NCs and 8.55 for MQ-GO/PEG NCs, further support the stability of the complexes in this (gas) phase.

In the aqueous environment, the miscibility between MQ and GO nanocarriers remained prominent, *albeit*, with slightly reduced chi values when compared to the gas phase. The MQ-GO NCs complex exhibited a chi value of 9.50, while the MQ-GO/PEG NCs complex, showed a lower value of 1.36. Despite this decrease, both systems still demonstrated considerable miscibility, as evidenced by their E_{mix} values of 5.62 and 0.80, respectively.

Similar trends, in miscibility, were observed in the acidic and alkaline phases, with relatively high chi values for both the MQ-GO NCs and MQ-GO/PEG NCs complexes. In the acidic phase, the MQ-GO NCs and MQ-GO/PEG NCs exhibited chi values of 15.01 and 6.59, respectively, along with E_{mix} values of 8.89 and 3.90. Conversely, in the alkaline phase, considerably higher chi values of 28.47 for MQ-GO NCs and 26.54 for MQ-GO/PEG NCs

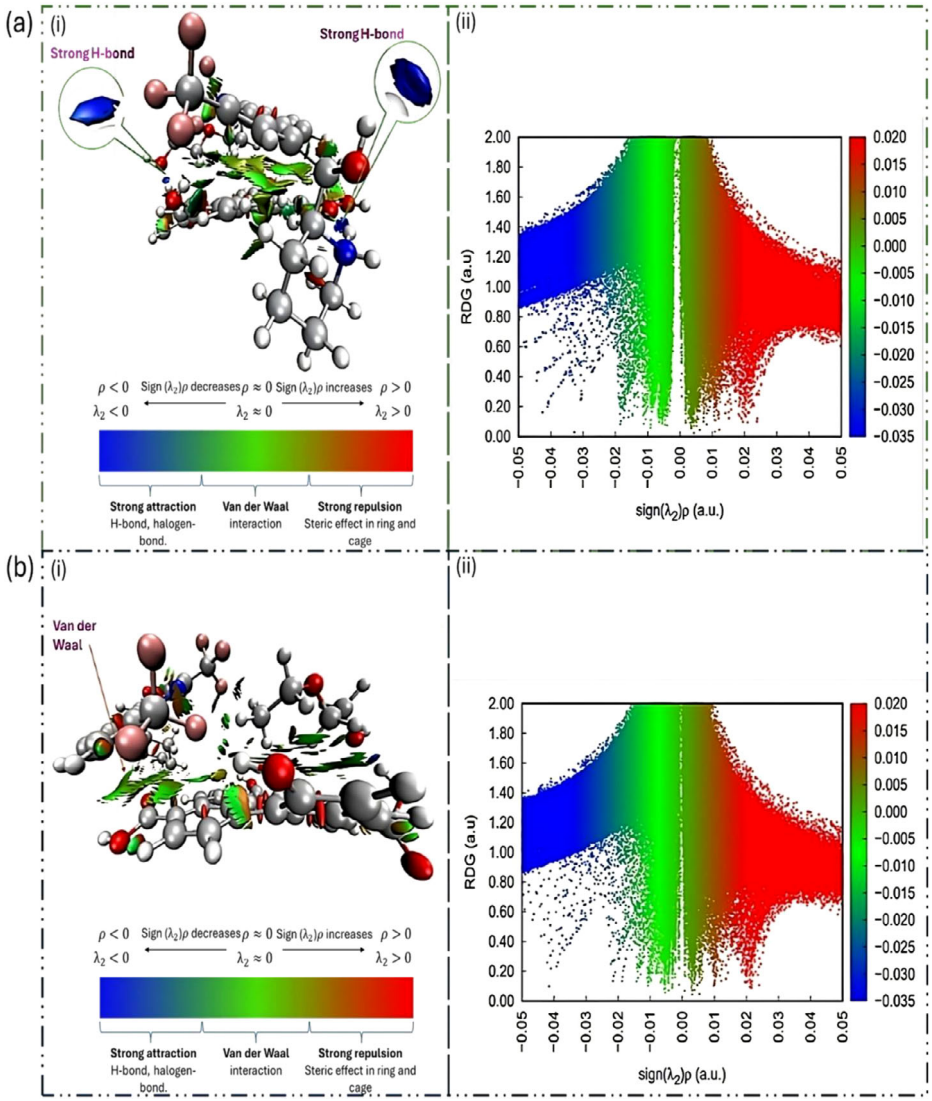

Figure 6. Exploration of the noncovalent interactions within the optimized MQ-GO/PEG NCs complex via RDG isosurface mapping (left) and the scatter plot analysis (right) across: a) acid and b) alkaline phases, offering an insight into the intermolecular forces and the molecular recognition patterns.

were recorded, with corresponding E_{mix} values of 16.86 and 15.71. These results indicate favorable interactions between MQ and GO nanocarriers across a wide pH range, underscoring their potential utility in diverse physiological conditions.

Figure 7 illustrates the temperature-dependence of the chi interaction parameter for both the MQ-GO NCs and MQ-GO/PEG NCs complexes, across different phases. The trends depicted in the graph (Figure 7), highlight the influence of temperature on the miscibility of MQ drug-GO nanocarrier systems, hence, providing valuable insights into their thermodynamic behaviors. However, in general, the curves for the MQ-GO NCs complex, exhibit higher chi (χ) values when compared to the MQ-GO/PEG NCs complex, indicating stronger interaction between MQ and GO nanocarriers without PEGylation.

Figure 8 and Figure S5 (Supporting Information) elucidate the binding configurations of the MQ-GO/PEG NCs and MQ-GO NCs complexes in the various phases under study, thereby offering a visual representation of the molecular interactions between MQ and GO nanocarriers. These configurations provide essential structural insights into the stability and efficacy of the drug delivery systems under investigation.

It can be inferred that the findings of this miscibility study contribute significantly to the understanding of Mefloquine delivery when utilizing PEGylated GO nanocarriers across different phases. The demonstrated miscibility and stability of the MQ drug-GO nanocarrier complexes underscore the potential of these systems for targeted drug delivery applications. Moreover, the versatility of these nanocarriers in accommodating diverse pH conditions enhances their potential relevance for antiviral treatment, where effective drug delivery to specific cellular targets, is paramount. By leveraging the favorable interactions elucidated in this study, researchers can potentially optimize the design of nanocarrier-based drug delivery systems for enhanced therapeutic outcomes in various clinical settings.

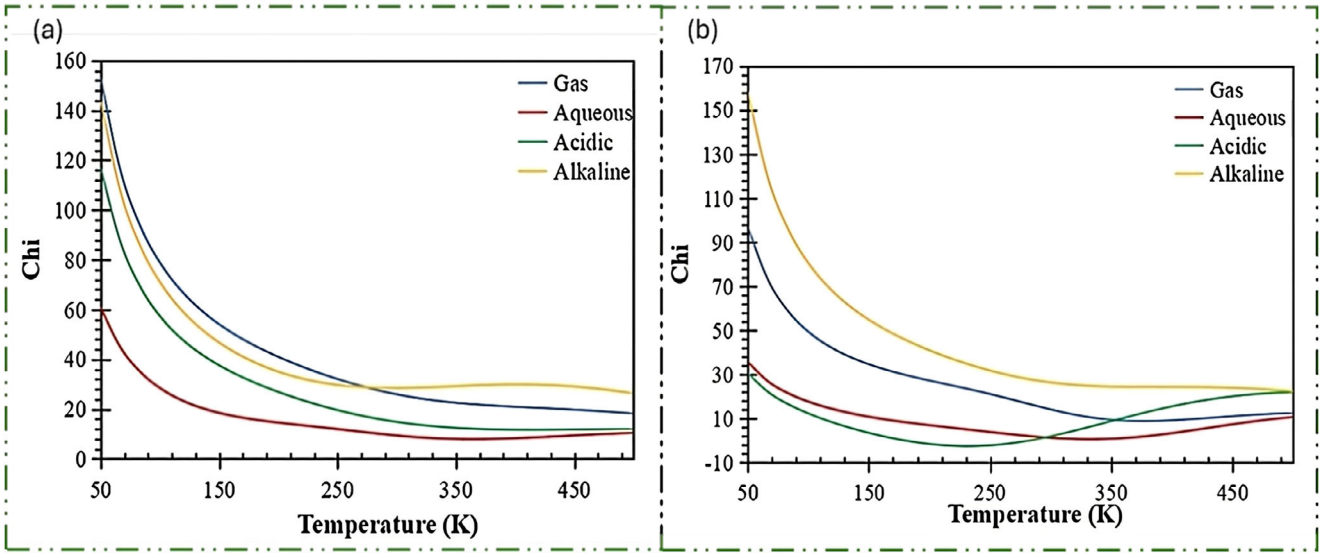

Figure 7. Graphical representation of the chi interaction parameter, plotted against temperature for: a) MQ-GO NCs and b) MQ-GO/PEG NCs complexes, explored across the various phases under study, unveiling temperature-dependent interactions and thermodynamic stability dynamics.

3.3. Release Mechanism of the MQ Drug-GO Nanocarrier Systems

The release mechanisms of the MQ drug-GO nanocarrier systems, shed light on the dynamics of drug release, influenced by the adsorption energy (E_{ad}) of the drug on the GO-based nanocarriers. The analysis of these systems plays a pivotal role in refining the drug delivery mechanisms and the investigation of their possible uses, specifically for antiviral therapy.

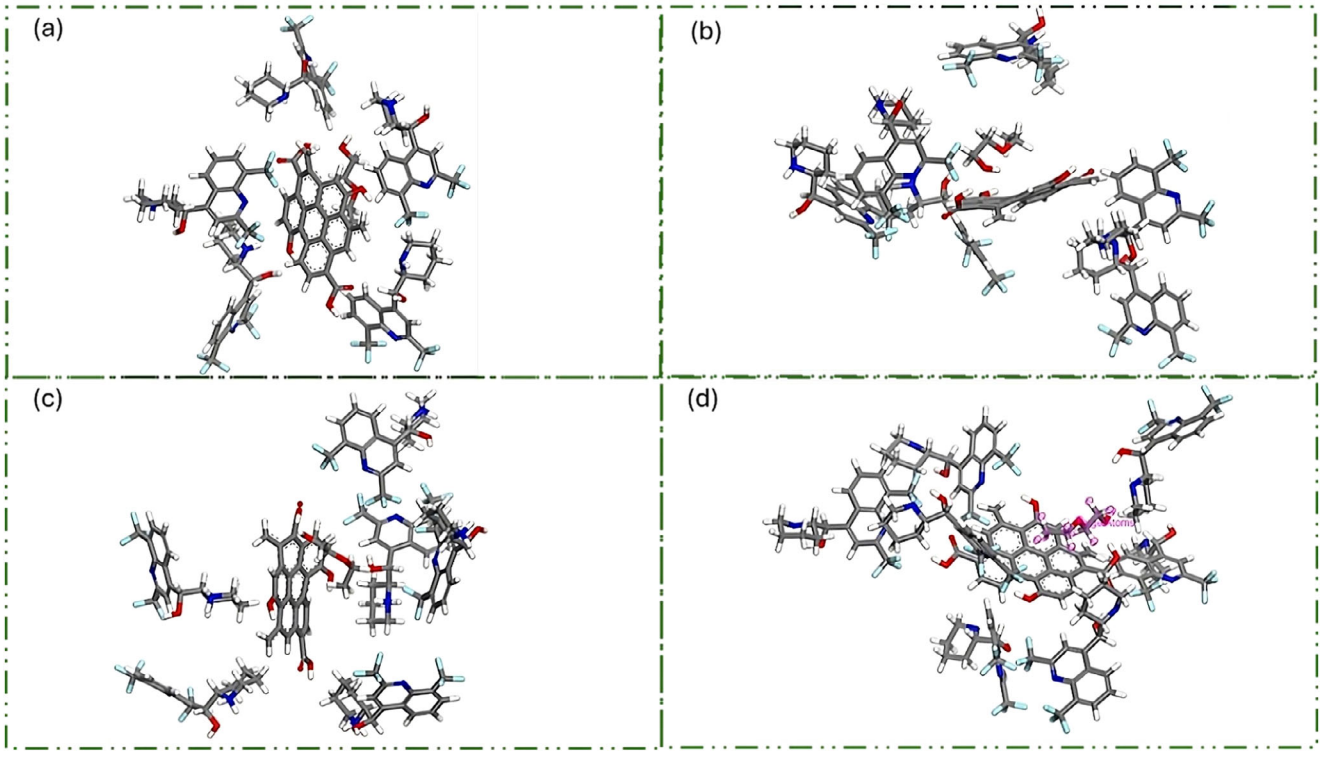

Figure 8. Visualization of the binding configuration of the MQ-GO/PEG NCs complex in a) gas, b) aqueous, c) acidic, and d) alkaline phases, offering insight into a molecular arrangement and interactions under diverse environmental conditions.

The release time (τ) of the drug from the GO nanocarriers, is determined by Equation 5, where the higher adsorption energies, correspond to longer release times. Specifically,

$$\tau = \nu_0^{-1}\, exp\left(\frac{-E_b}{KT}\right) \quad (5)$$

where T represents the temperature (in Kelvin, K), k denotes Boltzmann's constant, and ν_0 stands for the frequency of the attempt. When utilizing the UV light for this application, the value of ν_0 at room temperature, was found to be 10^{12}.[23]

In Table 1, the release time (τ) of the drug from the GO nanocarriers, is summarized across the various phases. It is noteworthy that any release time greater than 10^8 ms indicate prolonged release, rendering the system unsuitable for drug release at the target site due to the extended duration.

Meanwhile, in the gas phase, both the MQ-GO NCs and MQ-GO/PEG NCs complexes exhibit remarkably prolonged release times, with τ values in the order of 10^{35} to 10^{72} ms. This indicates significant adsorption of energy between MQ and the nanocarriers, leading to a slow release of the drug molecules.

Going from the gaseous to the aqueous state, the release times decrease when compared to the gas phase but remain in the range of between 10^{30} to 10^{66} ms. The presence of water molecules affects the drug-nanocarrier interactions, influencing the release kinetics of MQ from the complexes.

Under acidic conditions, the release times exhibit a wide range from 10^{63} to 10^{91} ms, indicating varying degrees of drug release kinetics. The acidic environment may modulate the adsorption energy between MQ and the nanocarriers, thereby affecting the drug release dynamics.

In alkaline environments, the release times range from 10^{43} to 10^{61} ms, demonstrating prolonged release kinetics like those observed in other phases. The alkaline pH environment may further influence the interactions between MQ and the nanocarriers, impacting the drug release behavior.

The observed recovery time for the MQ desorption from the nanocarriers is generally, higher when compared to the recovery time for Favipiravir from PAMAM (9.2×10^3 s) and polyester (4.2×10^3 s).[21,24] While the inherent characteristics of the GO nanocarriers offer advantages, such as high surface area and tunable surface chemistry, the prolonged release kinetics observed across the various phases, highlight the need for further refinement. Strategies, such as surface modification, functionalization, or incorporation of stimuli-responsive elements could be explored to achieve controlled and targeted drug release.

The findings with respect to the release mechanism of MQ from GO nanocarriers, provide valuable insights into the challenges associated with achieving efficient drug release across different phases. The prolonged-release times observed, underscore the importance of optimizing the design of nanocarrier-based drug delivery systems to enhance release kinetics and improve the therapeutic efficacy of the systems.

3.4. Thermodynamics of the MQ Drug-GO Nanocarrier Systems

In this section, we delve into the thermodynamic aspects of MQ drug transport using PEGylated GO nanocarriers across the various phases studied. **Table 2** offers insights into the energy parameters of the different drug-excipient species in these phases, focusing on the enthalpy (ΔH) and the Gibbs free energy (ΔG) values at 298.15 Kelvin (K).

In the gas phase, the calculated values of the ΔG and ΔH for the MQ-GO NCs and MQ-GO/PEG NCs complexes, indicate favorable interactions between MQ and GO nanocarriers. Both the MQ-GO NCs and MQ-GO/PEG NCs complexes, exhibit negative ΔG values, signifying spontaneous processes, with the ΔH values, reflecting exothermic interactions. Notably, the ΔG and ΔH values for MQ-GO NCs and MQ-GO/PEG NCs complexes in the gas phase are substantially, lowered when compared to aqueous, acidic, and alkaline phases, suggesting relatively weaker interactions in gaseous environments. Specifically, the enthalpy heat changes (ΔH) for the MQ-GO NCs and MQ-GO/PEG NCs complexes, are −114.94 and −65.417 Kcal mol^{-1}, respectively.

Within the aqueous phase, the calculated ΔG and ΔH values for the MQ-GO NCs and MQ-GO/PEG NCs complexes remain negative, indicating favorable interactions between the MQ and GO nanocarriers. However, the magnitudes of ΔG and ΔH are slightly higher when compared to the gas phase, suggesting stronger interactions in aqueous environments. Notably, the MQ-GO NCs complex, exhibits higher negative ΔG and ΔH values when compared to the MQ-GO/PEG NCs complex in the aqueous phase, indicating potentially, enhanced stability of MQ-GO NCs complexes in water. The enthalpy heat changes for the MQ-GO NCs and MQ-GO/PEG NCs complexes are −107.73 and −60.33 Kcal mol^{-1}, respectively.

In both the acidic and alkaline phases, the calculated ΔG and ΔH values, further underscore the favorable interactions between MQ and GO nanocarriers. Despite the variations in the magnitude of the ΔG and ΔH values among the different systems, negative values are observed for all complexes, indicating spontaneous and exothermic processes. Interestingly, the ΔG and ΔH values for the MQ-GO NCs and MQ-GO/PEG NCs complexes, in the acidic and alkaline phases, exhibit trends like those in the aqueous phase, *albeit*, with some variations, suggesting differential energetics in the acidic and alkaline media.

The favorable thermodynamic parameters observed suggest that the PEGylated GO nanocarriers have the potential to efficiently encapsulate Mefloquine, enhancing its solubility and stability in the various environments under study. This is particularly crucial in antiviral treatment, where effective drug delivery systems can improve the bioavailability and efficacy of antiviral medications like Mefloquine. Additionally, the exothermic nature of the complex formation process implies the fact that the release of Mefloquine from the nanocarriers could be controlled, allowing for sustained and targeted drug delivery, which is beneficial in managing viral infections.

3.5. Electronic and Quantum Chemical Descriptors of the MQ Drug-GO Nanocarrier Systems

In this section, we elucidate the electronic and quantum chemical descriptors of the MQ drug-GO nanocarrier systems, shedding light on their behaviors across different phases and their implications for drug delivery, with a specific focus on Mefloquine transport by using PEGylated GO nanocarriers.

Table 2. Comprehensive analysis of the thermodynamic energy parameters for diverse drug-excipient species across varied phases, elucidating the interactions, and stability dynamics that are critical for pharmaceutical formulation developments.

Species	E_{tot} [Ha]	$H^{298.15}_{TCorr}$ [Ha]	$G^{298.15}_{TCorr}$ [Ha]	$\Delta H^{298.15K}$ [Kcal/mol]	$\Delta G^{298.15K}$ [Kcal/mol]
Gas					
MQ	−1525.74	−1525.40	−1525.47	–	–
GO	−1538.75	−1538.39	−1538.47	–	–
GO/PEG	−1865.58	−1865.07	−1865.16	–	–
MQ-GO NCs	−3064.67	−3063.97	−3064.09	−114.94	−98.25
MQ-GO/PEG NCs	−3391.425	−3390.57	−3390.71	−65.417	−50.34
Aqueous					
MQ	−1525.76	−1525.42	−1525.49	–	–
GO	−1538.78	−1538.42	−1538.50	–	–
GO/PEG	−1865.62	−1865.11	−1865.20	–	–
MQ-GO NCs	−3064.71	−3064.01	−3064.13	−107.73	−90.82
MQ-GO/PEG NCs	−3391.47	−3390.62	−3390.76	−60.33	−42.17
Acidic					
MQ	−1526.24	−1525.89	−1525.96	–	–
MQ-GO NCs	−3065.22	−3064.50	−3064.63	−142.82	−124.75
MQ-GO/PEG NCs	−3391.99	−3391.12	−3391.26	−102.76	−84.30
Alkaline					
MQ	−1525.10	−1524.77	−1524.85	–	–
MQ-GO NCs	−3063.82	−3063.13	−3063.25	22.79	41.07
MQ-GO/PEG NCs	−3390.53	−3389.69	−3389.83	96.72	113.98

The frontier molecular orbital analysis provides crucial insights into the spatial distribution of the highest occupied molecular orbital (HOMO) and the lowest unoccupied molecular orbital (LUMO) within the MQ drug-GO complexes and across various phases. The 3D representations of the frontier molecular orbitals, as depicted in **Figure 9** and Figure S6 (Supporting Information), offer visual insights into the electron density distribution and bonding interactions within the MQ-GO/PEG NCs and MQ-GO NCs complexes and across the various phases studied. Understanding the FMOs is helpful in elucidating the electronic structures and reactivities of the nanocarrier-drug complexes. In the gas and water phases, both the MQ-GO NCs and MQ-GO/PEG NCs complexes exhibit HOMO and LUMO, predominantly residing on the GO structure. However, intriguing variations occur in acidic and alkaline environments. In the acidic phase, the HOMO shifts to the edges of the GO, while the LUMO localizes on the MQ molecule. Conversely, in the alkaline phase, the HOMO is observed on the MQ molecule, with the LUMO distributed across both the MQ drug and the GO structure. This alteration suggests variations in the charge transfer processes and the molecular stability under different pH conditions, which could influence the drug release kinetics and efficacy. The energy gap (E_g) between the HOMO and LUMO serves as a crucial parameter indicating the electronic properties of the nanocarriers. The incorporation of the MQ drug induces alterations in the E_g, and hence, influencing the electrical conductivity of the complexes. Notably, significant changes in E_g occur across the different phases, with the percentage change in the energy gap (%ΔE_g) ranging from −80.89% to 3.95%.

The introduction of MQ to GO, results in a reduction of the energy gap (ΔEg) when compared to the individual components. Furthermore, the addition of PEG to GO (GO/PEG) marginally affects the energy gap, indicating a minimal alteration in the electronic structure when compared to GO alone.

Moving beyond the gas phase, the behavior of the MQ drug-GO nanocarrier systems in aqueous, acidic, and alkaline environments, reveals intriguing trends. For instance, in water, the introduction of MQ to GO leads to a reduction in the energy gap, suggesting potential enhancements in reactivity and interaction between the drug and the carrier. Notably, the inclusion of PEGylation further decreases the energy gap, indicating improved compatibility and stability in aqueous environments.

In acidic conditions, the electronic properties of the nanocarrier systems undergo significant changes. For instance, while MQ exhibits a relatively stable energy gap, the presence of GO and PEGylated GO alters the E_{HOMO} and E_{LUMO} levels, thereby potentially influencing the drug's release kinetics and efficacy in acidic environments. Similarly, in alkaline conditions, the electronic properties of the nanocarrier systems are substantially modified, with implications for drug delivery efficiency and stability. These variations underscore the sensitivity of the nanocarriers to environmental factors and drug interactions, highlighting their potential for controlled drug release and tailored/targeted delivery strategies.[23e,25]

Quantum descriptors (**Table 3**) provide further insights into the electronic properties of the complexes, including the electron affinity (η), chemical potential (μ), softness (s), and global hardness (ω) of the systems.[26] Across the gas phase, the MQ drug

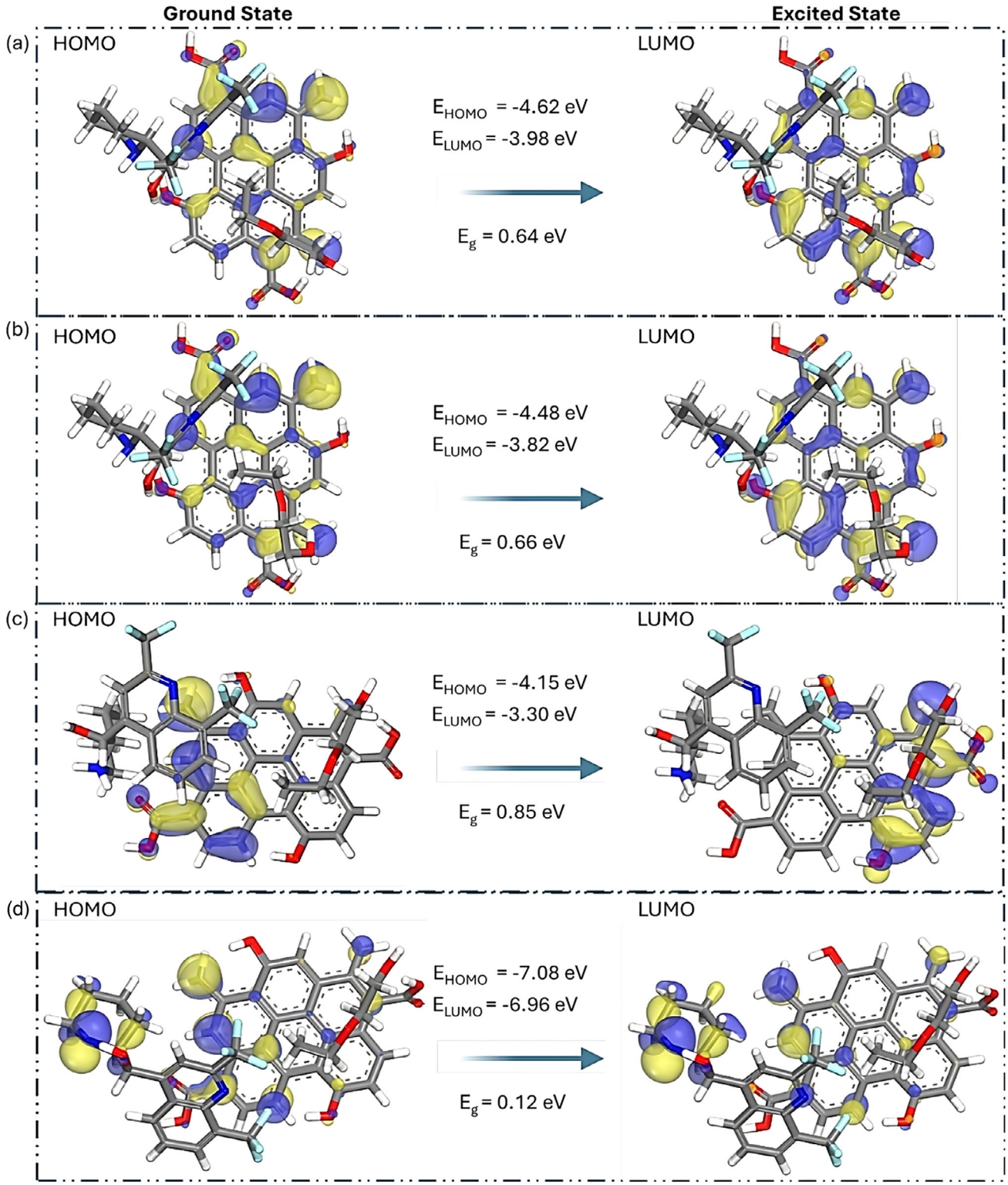

Figure 9. 3D visualization of the frontier molecular orbitals of the MQ-GO/PEG NCs complexes in: a) gas, b) aqueous c) acidic, and d) alkaline phases, showcasing the intricate electronic structure and spatial distribution that are critical for the understanding of the reactivity and stability of the drug-nanocarrier complexes across diverse environments.

Table 3. Quantum chemical descriptors of MQ-GO nanocarrier complexes in different phases, offering insights into the reactivity, stability, and electron transfer dynamics, critical for the understanding of drug delivery mechanisms and their potential for therapeutic applications.

Structure configuration	E_{HOMO} [eV]	E_{LUMO} [eV]	E_g [eV]	ΔE_g [%]	η [eV]	μ [eV]	s [eV]	ω [eV]	ECT
Gas									
MQ	−6.41	−2.51	3.90	–	1.95	−4.46	0.51	5.10	–
GO	−4.67	−4.02	0.65	–	0.33	−4.345	3.06	28.83	–
GO/PEG	−4.51	−3.86	0.64	–	0.32	−4.19	3.09	27.12	–
MQ-GO NCs	−4.70	−4.10	0.60	−8.93	0.30	−4.40	3.36	32.54	10.99
MQ-GO/PEG NCs	−4.62	−3.98	0.64	−0.93	0.32	−4.30	3.12	28.84	10.67
Water									
MQ	−6.19	−2.48	3.71	–	1.86	−4.34	0.54	5.06	–
GO	−4.60	−3.95	0.65	–	0.33	−4.28	3.06	27.96	–
GO/PEG	−4.51	−3.87	0.64	–	0.32	−4.19	3.13	27.50	–
MQ-GO NCs	−4.59	−3.97	0.61	−6.01	0.31	−4.28	3.26	29.78	10.75
MQ-GO/PEG NCs	−4.48	−3.82	0.66	3.95	0.33	−4.15	3.01	25.95	10.79
Acidic									
MQ	−5.58	−1.86	3.72	–	1.86	−3.72	0.549	3.72	–
MQ-GO NCs	−3.82	−2.74	1.08	65.37	0.54	−3.28	1.85	9.96	11.28
MQ-GO/PEG NCs	−4.15	−3.30	0.85	32.25	0.427	−3.73	2.34	16.24	10.96
Alkaline									
MQ	−7.15	−3.08	4.06	–	2.03	−5.11	0.49	6.44	–
MQ-GO NCs	−4.59	−4.17	0.42	−36.52	0.21	−4.38	4.82	46.23	10.76
MQ-GO/PEG NCs	−7.08	−6.96	0.12	−80.89	0.062	−7.02	16.19	398.84	10.44

exhibited a higher global softness (η) of 1.95 eV when compared to GO (0.33 eV), indicating its relatively higher reactivity. However, upon complex formation with GO, the η value decreased to 0.30 eV for the MQ-GO NCs and 0.32 eV for MQ-GO/PEG NCs. Similarly, the chemical potential (μ) of MQ (−4.46 eV) was higher than that of GO (−4.345 eV), indicating a higher electron donation ability. Upon complexation, the μ values decreased, suggesting a reduction in its electron donation ability. Furthermore, the chemical hardness (s) values of the complexes were generally, higher than those of the individual components, indicating increased stability upon complexation. In the aqueous phase, similar trends were observed, with MQ exhibiting higher η and μ values when compared to GO, and subsequent decreases upon complex formation. Notably, the addition of PEG to GO slightly, increased the hardness when compared to GO alone, suggesting an enhanced stability of the GO/PEG system. In acidic environments, the values of η, μ, and s varied significantly when compared to the gas and aqueous phases. In particular, the η value of MQ decreased, indicating a reduced reactivity, while the chemical hardness increased, suggesting an increased stability upon complexation with either GO or GO/PEG. In alkaline environments, the values of η and μ for MQ and the complexes showed distinct differences when compared to other phases. Notably, the electrophilicity index (ω) of MQ was significantly higher in the gas phase when compared to other configurations, indicating a higher electron-accepting ability, which decreased upon complex formation. These findings provide crucial insights into the interactions and properties of the MQ drug-GO nanocarrier complexes, hence, shedding more light on their behaviors, across different phases.[6a]

3.6. Theoretical IR and UV Spectra Analysis of the MQ Drug-GO Nanocarrier Systems

The vibrational fingerprints obtained from the IR spectra (**Figure 10**; Figure S7, Supporting Information), along with the corresponding wavenumbers and intensities, offer valuable information with respect to the nature and strength of molecular bonds and interactions. These spectroscopic techniques can provide valuable information about the molecular interactions, structural changes, and electronic transitions occurring within the drug-nanocarrier complexes across different phases.[6a,11]

In the gas phase, distinctive peaks were observed for both systems. For the MQ drug-GO nanocarrier system, prominent peaks were detected at wavenumbers of ≈1174.99, ≈1817.99, and ≈3730.49 cm^{-1}. These peaks correspond to the vibrational modes associated with specific functional groups. The peak at 1174.99 cm^{-1} can be attributed to C—O stretching, while the peak at 1817.99 cm^{-1}, represents the presence of C═O stretching. Additionally, the peak at 3730.49 cm^{-1} indicates the presence of N—H stretching vibrations, characteristic of the Mefloquine drug. Interestingly, the addition of PEGylation to the GO nanocarrier system resulted in shifts in the wavenumbers and changes in intensities, suggesting alterations in the molecular interactions and the bonding patterns.

Moving to aqueous media, the IR spectra revealed distinct peaks, indicative of altered molecular environments. In both systems, peaks at ≈1098.81, ≈1776.81, and ≈3687.81 cm^{-1}, were observed. These peaks correspond to the vibrations associated with different functional groups, i.e., C—O stretching and N—H stretching, characteristic of the MQ drug. Notably, the intensities

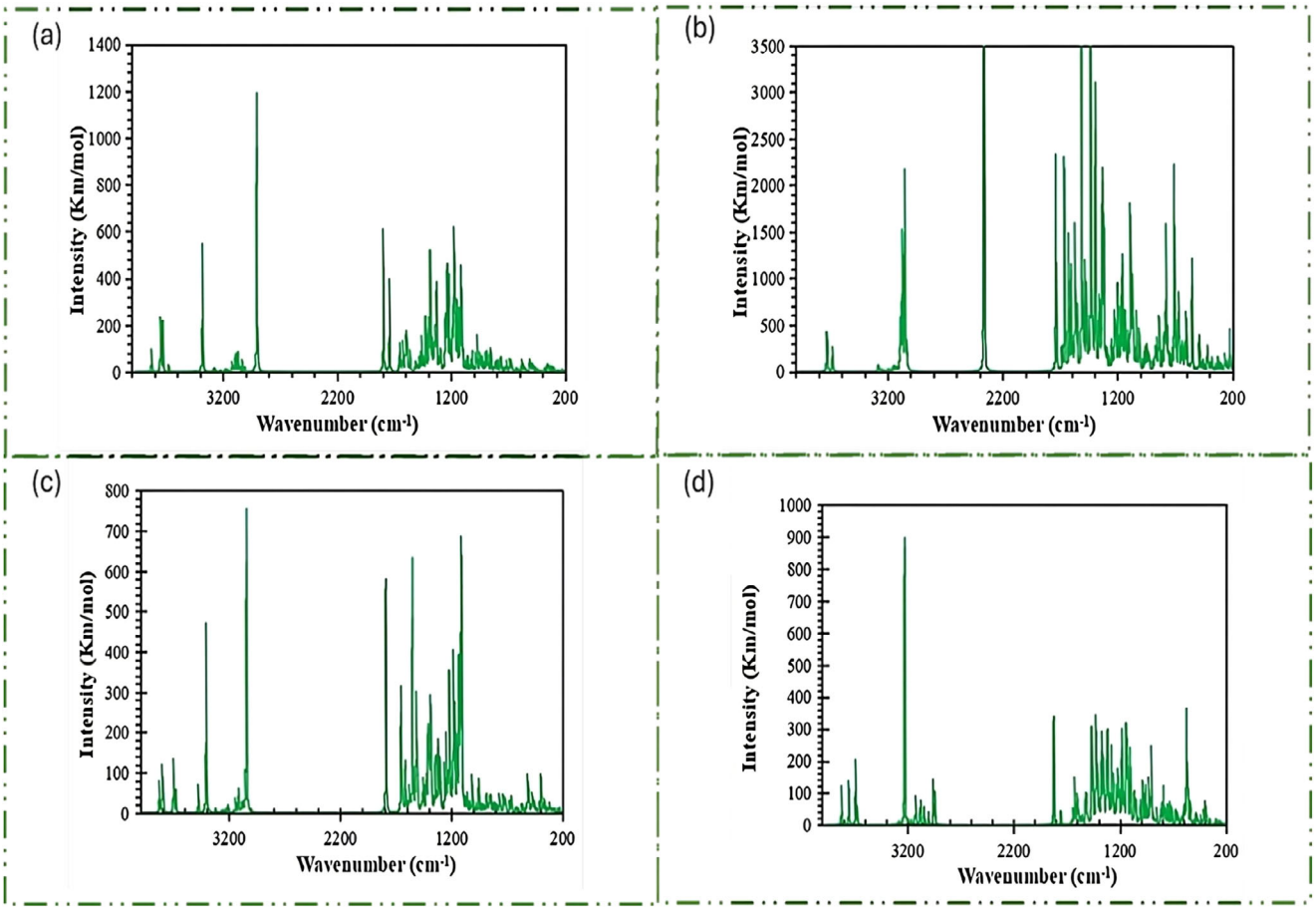

Figure 10. Infrared spectroscopy analysis of MQ-GO/PEG NCs complexes in: a) gas, b) aqueous, c) acidic, and d) alkaline phases, revealing the molecular vibrational fingerprints and the environmental influence on molecular interactions.

of these peaks varied, suggesting modifications in molecular interactions, influenced by the presence of water molecules.

In acidic and alkaline environments, significant shifts in wavenumbers and intensities were observed, indicating changes in molecular structures and interactions. In the acidic phase, peaks at ≈1691.99 and ≈2190.49 cm^{-1} were detected, representing distinctive vibrational modes that are associated with protonation and hydrogen bonding. Conversely, in the alkaline phase, peaks at 2451.75, 2721.75, 3154.75, and 3471.25 cm^{-1} were observed, indicating the influence of hydroxide ions on molecular vibrations and interactions.

These findings offer profound insights into the behavior of MQ drug-GO and MQ drug-PEGylated GO nanocarrier systems across different phases, shedding light on their potential for drug delivery applications. The alterations observed in the vibrational frequencies and intensities highlight the sensitivity of IR spectroscopy in detecting subtle changes in molecular environments and interactions.

Furthermore, we conducted UV spectra analysis to elucidate the interaction between MQ and GO nanocarriers, both with and without PEG modification, and across different phases, including gas and aqueous environments. The values of the excitation wavelength (λ_{max}) and oscillator strength (f), i.e., the dimensionless quantity that expresses the probability of absorption or emission of electromagnetic radiation in transitions between the energy levels of an atom or molecule, for each species, in the various phases studied, are presented in **Figure 11** and **Table 4**.

In the gas phase, both the MQ-GO NCs and MQ-GO/PEG NCs exhibited distinct UV spectra characteristics. For the MQ-GO NCs, two distinct excitation peaks were observed at ≈266.35 and 461.35 nm, corresponding to energy levels of 4.64 and 2.68 eV, respectively. The oscillator strengths for these peaks were 0.68 and 0.14, respectively. Conversely, MQ-GO/PEG NCs displayed a single excitation peak at 265.98 nm with an energy level of 4.66 eV and an oscillator strength of 1.20. These findings suggest differences in the electronic transitions and absorption characteristics between MQ-GO NCs and MQ-GO/PEG NCs in the gas phase.

In aqueousenvironments, the UV spectra of MQ-GO NCs and MQ-GO/PEG NCs showed shifts in the excitation peaks when compared to the gas phase. The excitation peaks were observed at ≈262.85 and ≈438.85 nm for MQ-GO NCs, with corresponding energy levels of 4.72 and 2.82 eV, and oscillator strengths of 0.55 and 0.10, respectively. For the MQ-GO/PEG NCs, a single excitation peak was observed at 261.25 nm with an energy level of 4.74 eV and an oscillator strength of 1.11. These shifts indicate changes in the electronic structure and interactions of the drug-nanocarrier complexes in aqueous environments when compared to the gas phase.

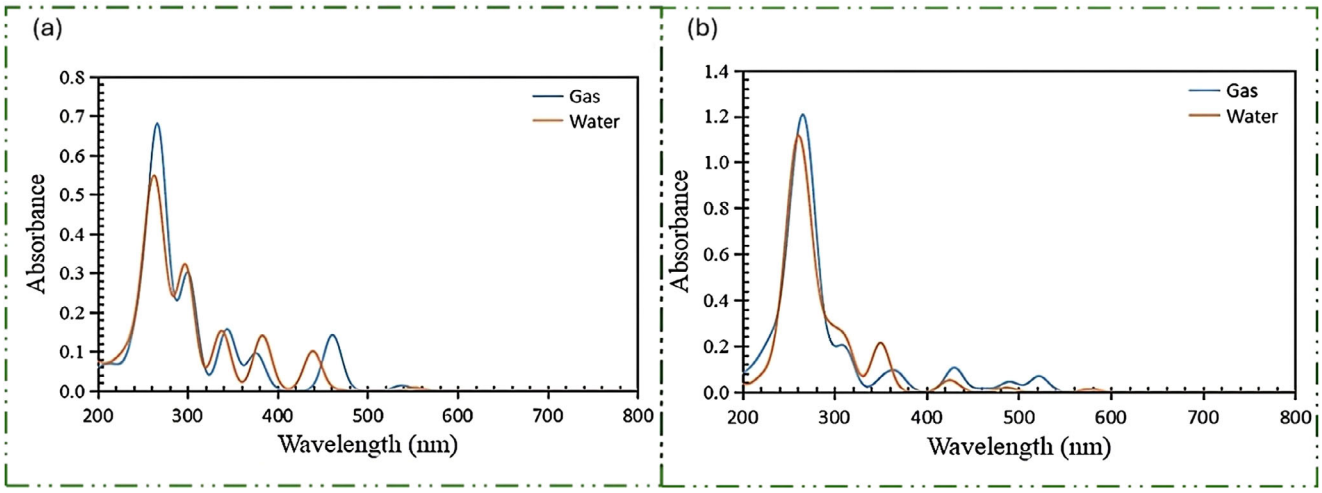

Figure 11. UV spectroscopy analysis of the: a) MQ-GO NCs and b) MQ-GO/PEG NCs complexes in gas, and aqueous phases, highlighting the absorption spectra and the molecular interactions underpinning the drug-nanocarrier interactions in different environments.

4. Conclusion

This study investigated the *in-silico* transport of MQ, a potent antimalarial and antiviral drug, by using GO and GO/PEGylated graphene oxide (GO/PEG) nanocarriers, across various phases and environmental conditions. The results revealed the following key findings:

1) Interaction and stability: MQ exhibited a strong affinity and favorable interactions with GO and GO/PEG nanocarriers, especially in acidic environments, indicating enhanced stability and potential for targeted drug delivery. The adsorption energies ranged from −59.14 to −143.16 kcal moℓ^{-1}, while the adsorption distances ranged from 1.50 to 2.50 Å.
2) Miscibility and thermodynamics: MQ and GO nanocarriers demonstrated good miscibility across different phases, as evidenced by the chi interaction parameter and the energy of the mixture. The thermodynamic parameters, e.g., enthalpy and the Gibbs free energy, indicated spontaneous and exothermic processes upon complex formation, implying a controlled and sustained drug release.
3) Electronic and quantum properties: MQ and GO nanocarriers exhibited distinct electronic and quantum properties, influenced by environmental factors and drug interactions. The frontier molecular orbital analysis showed variations in the HOMO and LUMO levels, thereby affecting the charge transfer and the reactivity of the complexes. The quantum descriptors, such as: electron affinity, chemical potential, softness, and hardness, reflected the stability and electron transfer dynamics of the complexes.
4) Release kinetics: MQ and GO nanocarriers displayed prolonged release times across different phases, indicating significant adsorption energy and slow drug release. The release times ranged from 12.03×10^{30} to 6.98×10^{91} ms, suggesting the need for further optimization of the nanocarrier systems to enhance release kinetics and therapeutic efficacy.

In summary, this study has provided valuable insights into the molecular interactions and mechanisms underlying MQ transport by using GO and GO/PEG nanocarriers across diverse environments. The findings suggested the potential of these nanocarrier systems for efficient and targeted drug delivery, with applications reaching beyond malaria treatment. Further studies are needed to validate the *in-silico* results and to explore the optimal design and performance of these nanomedicines, in-vivo.

Table 4. UV spectroscopic parameters characterizing MQ-GO NCs and MQ-GO/PEG NCs complexes across gas and aqueous phases, providing a comprehensive insight into the absorption characteristics and molecular dynamics governing drug-nanocarrier interactions.

Species	Phases	Level Energy [eV]	Excitation [λ_{max}]	Oscillator strength [f]
MQ-GO NCs	gas	4.64*	266.35	0.68
		2.68*	461.35	0.14
	water	4.72	262.85	0.55
		2.82	438.85	0.10
MQ-GO/PEG NCs	gas	4.66*	265.98	1.20
	water	4.74	261.25	1.11

Supporting Information

Supporting Information is available from the Wiley Online Library or from the author.

Acknowledgements

O.C.A. and G.J.A. would like to thank the Center for High Performance Computing (CHPC), South Africa for access to computing resources. Additionally, OCA lovingly appreciates his wife, Omolola Felicia Adekoya, while GJA expresses heartfelt gratitude and paternal affection toward his beloved daughter, Oluwaferanmi Tiara Adekoya.

Conflict of Interest

The authors declare no conflict of interest.

Author Contributions

O.C.A. and G.J.A. performed software, data curation, conceptualization, methodology, formal analysis. Y.H. and E.R.S. performed supervision, validation and writing-reviewed and edited the final manuscript.

Data Availability Statement

The data that support the findings of this study are available from the corresponding author upon reasonable request.

Keywords

DFT, drug delivery, graphene oxide, mefloquine, nanomedicine, polyethylene glycol

Received: May 14, 2024
Revised: June 13, 2024
Published online: September 1, 2024

[1] a) O. C. Adekoya, M. E. Yibowei, G. J. Adekoya, E. R. Sadiku, Y. Hamam, S. S. Ray, *Mater. Today: Proceedings* **2022**, *62*, S141; b) G. J. Adekoya, A. C. Ezika, O. C. Adekoya, E. R. Sadiku, Y. Hamam, S. S. Ray, *BMEMat.* **2023**, *1*, e12042.

[2] a) J. Karbwang, N. J. White, *Clin. Pharmacokinet.* **1990**, *19*, 264; b) K. J. Palmer, S. M. Holliday, R. N. Brogden, *Drugs* **1993**, *45*, 430.

[3] a) M. Gendrot, I. Duflot, M. Boxberger, O. Delandre, P. Jardot, M. L.e Bideau, J. Andreani, I. Fonta, J. Mosnier, C. Rolland, S. Hutter, B. L.a Scola, B. Pradines, *Inter. J. Infect. Diseases* **2020**, *99*, 437; b) K. Shionoya, M. Yamasaki, S. Iwanami, Y. Ito, S. Fukushi, H. Ohashi, W. Saso, T. Tanaka, S. Aoki, K. Kuramochi, *Frontiers in Microbiology* **2021**, *12*, 989.

[4] a) M. Taher, S. S. Shaari, D. Susanti, *Journal of Pharmacy* **2021**, *1*, 34; b) C. Shi, Z. Zhang, J. Shi, F. Wang, Y. Luan, *Int. J. Pharm.* **2015**, *495*, 932.

[5] a) D. Bhadra, S. Bhadra, N. K. Jain, *IEEE*, **2004**, 353; b) D. Bhadra, S. Bhadra, N. K. Jain, *Pharm. Res.* **2006**, *23*, 623.

[6] a) O. C. Adekoya, G. J. Adekoya, R. E. Sadiku, Y. Hamam, S. S. Ray, *ACS Omega* **2022**, *7*, 33808; b) A. Angelopoulou, E. Voulgari, E. K. Diamanti, D. Gournis, K. Avgoustakis, *Eur. J. Pharm. Biopharm.* **2015**, *93*, 18; c) J. Charmi, H. Nosrati, J. M. Amjad, R. Mohammadkhani, H. Danafar, *Heliyon* **2019**, *5*, e01466.

[7] H. Wen, C. Dong, H. Dong, A. Shen, W. Xia, X. Cai, Y. Song, X. Li, Y. Li, D. Shi, *Small* **2012**, *8*, 760.

[8] M. Kazempour, H. Namazi, A. Akbarzadeh, R. Kabiri, *Artif. Cells, Nanomed., Biotechnol.* **2019**, *47*, 90.

[9] a) M. A. Jihad, F. T. M. Noori, M. S. Jabir, S. Albukhaty, F. A. AlMalki, A. A. Alyamani, *Molecules* **2021**, *26*, 3067; b) S. Karimi, H. Namazi, *J. Alloys Compd.* **2021**, *879*, 160426.

[10] a) K. M. Alharthy, M. F. Alsaffar, H. N. Althurwi, F. F. Albaqami, R. R. Abass, A. M. Alawi, S. S. Jalal, S. Tabassum, H. Zhang, W. Peng, *Inorg. Chem. Commun.* **2023**, *150*, 110482; b) M. Rana, P. Yadav, S. Lakhera, P. Chowdhury, **2023**; c) H. A. Naser, S. M. Merdas, F. H. Hanoon, A. N. Hussien, *HIV Nursing* **2023**, *23*, 1028; d) P. Ranjan, T. Chakraborty, *Theor. Chem. Acc.* **2023**, *143*, 7.

[11] O. C. Adekoya, G. J. Adekoya, E. R. Sadiku, Y. Hamam, S. S. Ray, *Pharmaceutics* **2022**, *14*, 1972.

[12] P. Swietach, R. D. Vaughan-Jones, A. L. Harris, A. Hulikova, *Philos Trans R Soc Lond B Biol Sci.* **2014**, *369*, 20130099.

[13] a) D. W. Boukhvalov, D. R. Dreyer, C. W. Bielawski, Y.-W. Son, *ChemCatChem* **2012**, *4*, 1844; b) A. Berisha, *J. Chem.* **2019**, *2019*, 5126071.

[14] a) B. Delley, *J. Chem. Phys.* **1990**, *92*, 508; b) B. Delley, *J. Chem. Phys.* **2000**, *113*, 7756.

[15] a) A. Klamt, G. Schüürmann, *J. Chem. Soc.* **1993**, *2*, 799; b) H. Xu, L. Li, G. Fan, X. Chu, *Comput. Theor. Chem.* **2018**, *1131*, 57.

[16] a) F. Mollarasouli, N. Zare-Shehneh, M. Ghaedi, *Microchim. Acta* **2022**, *189*, 103; b) R. Yapasert, P. Khaw-On, R. Banjerdpongchai, *Molecules* **2021**, *26*, 7459.

[17] T. Lu, F. Chen, *J. Comput. Chem.* **2012**, *33*, 580.

[18] W. Humphrey, A. Dalke, K. Schulten, *J. Mol. Graph.* **1996**, *14*, 33.

[19] Ü. Çalişir, Y. Camadan, B. Çiçek, E. Akkemik, V. Eyüpoğlu, Ş. Adem, *J. Biomol. Struct. Dyn.* **2023**, *41*, 1828.

[20] S. Grimme, *Wiley Interdiscip. Rev. Comput. Mol. Sci.* **2011**, *1*, 211.

[21] S. Bazyari-Delavar, F. Badalkhani-Khamseh, A. Ebrahim-Habibi, N. L. Hadipour, *J.Nanoparticle Res.* **2021**, *23*, 231.

[22] Z. H. Al-Sawaff, S. S. Dalgic, F. Kandemirli, M. Monajjemi, F. Mollaamin, *Russ. J. Phys. Chem. A* **2022**, *96*, 2953.

[23] a) A. Hosseinian, E. Vessally, A. Bekhradnia, K. Nejati, G. Rahimpour, *Thin Solid Films* **2017**, *640*, 93; b) R. Bagheri, M. Babazadeh, E. Vessally, M. Es'haghi, A. Bekhradnia, *Inorg. Chem. Commun.* **2018**, *90*, 8; c) S. Onsori, E. Alipour, *J. Mol. Graph.* **2018**, *79*, 223; d) K. Nejati, A. Hosseinian, E. Vessally, A. Bekhradnia, L. Edjlali, *Appl. Surf. Sci.* **2017**, *422*, 763; e) M. Wang, C. Tang, *Silicon* **2021**, *14*, 5463.

[24] T. d Silva Arouche, A. F. Reis, A. Y. Martins, J. F. S. Costa, R. N. Carvalho Junior, A. M. Jc Neto, *J. Nanosci. Nanotechnol.* **2020**, *20*, 7311.

[25] C. Xiao, K. Ma, G. Cai, X. Zhang, E. Vessally, *J. Mol. Graph.* **2020**, *96*, 107539.

[26] R. Rahimi, M. Solimannejad, *Appl. Surf. Sci.* **2020**, *525*, 146577.